EUROPEAN ORGANIZATION FOR NUCLEAR RESEARCH (CERN)

CERN-EP-2022-233
2022/11/25

CMS-HIG-21-012

Search for boosted Higgs boson decay to a charm quark-antiquark pair in proton-proton collisions at $\sqrt{s} = 13\,\text{TeV}$

The CMS Collaboration

Abstract

A search for the standard model (SM) Higgs boson (H) produced with transverse momentum greater than 450 GeV and decaying to a charm quark-antiquark ($c\bar{c}$) pair is presented. The search is performed using proton-proton collision data collected at $\sqrt{s} = 13\,\text{TeV}$ by the CMS experiment at the LHC, corresponding to an integrated luminosity of $138\,\text{fb}^{-1}$. Boosted $H \to c\bar{c}$ decay products are reconstructed as a single large-radius jet and identified using a deep neural network charm tagging technique. The method is validated by measurement of the $Z \to c\bar{c}$ decay process, which is observed with a signal strength of $1.00^{+0.17}_{-0.14}\,(\text{syst}) \pm 0.08\,(\text{theo}) \pm 0.06\,(\text{stat})$, defined as the ratio of the observed process rate to the standard model expectation. The observed (expected) upper limit on $\sigma(H)\,\mathcal{B}(H \to c\bar{c})$ is set at 47 (39) times the SM prediction at 95% confidence level.

Submitted to Physical Review Letters

The standard model (SM) Higgs boson (H) has been observed at the LHC [1–3] in all its expected primary production modes and most of its dominant decay channels. With the observations of direct couplings to τ leptons [4, 5], top quarks [6, 7], and bottom quarks [8, 9] confirming that the SM Yukawa sector gives rise to the masses of third-generation fermions, attention naturally turns to probing the second generation, specifically muons and charm quarks.

The search for H decays to muon pairs is the most experimentally accessible channel, and has been explored by the ATLAS [10, 11] and CMS [12] Collaborations. The latter recently found evidence of the H coupling to muons [13].

In contrast, the search for H decays to charm quark-antiquark pairs ($\mathrm{H} \to \mathrm{c\bar{c}}$) is considerably more challenging, because of the difficulty of identifying such decays and enormous multijet backgrounds. However, recent advances in jet substructure and flavor tagging techniques [14] have greatly improved the experimental sensitivity to this decay mode. Prior searches by the ATLAS [15, 16] and CMS [17, 18] have focused on H production in association with a vector boson (VH, where V stands for a W or Z boson), which benefits from strong background rejection thanks to leptonic decays of the vector bosons. The gluon-gluon fusion (ggF) and vector boson fusion (VBF) production modes have larger cross sections, but have yet to be explored.

This letter reports on the first search for the $\mathrm{H} \to \mathrm{c\bar{c}}$ decay at the LHC, where the H is produced with transverse momentum (p_T) greater than 450 GeV, enriched in events from the ggF production. The search employs the same general strategy as earlier CMS searches for boosted H in the $\mathrm{b\bar{b}}$ decay channel [19, 20], but uses new mass decorrelated discriminators to define a charm-enriched signal region. This search strategy provides an additional constraint on the decay process to the existing ATLAS and CMS measurements, in terms of production mode and H p_T.

The search is performed using a dataset of proton-proton collisions at $\sqrt{s} = 13\,\mathrm{TeV}$, collected with the CMS detector at the LHC, and corresponding to an integrated luminosity of $138\,\mathrm{fb}^{-1}$. Candidate events are selected by requiring a high-p_T, large-radius jet with substructure observables compatible with those expected from an $\mathrm{H} \to \mathrm{c\bar{c}}$ decay. Deep neural network (DNN) discriminators are employed to separate the H signal events from the dominant background, specifically quantum chromodynamics (QCD)-induced multijet events. The discriminators are designed to be independent of jet mass, which allows for both an estimation of the QCD background from control samples in data and for the validation of the analysis procedure through a search for $\mathrm{Z} \to \mathrm{c\bar{c}}$ decays. A model of the jet mass distributions for the $\mathrm{H} \to \mathrm{c\bar{c}}$ and $\mathrm{Z} \to \mathrm{c\bar{c}}$ signals, QCD multijet events, and other background processes is fit simultaneously in several disjoint signal and control regions to extract the signal production cross sections.

The CMS apparatus [21] is a multipurpose, nearly hermetic detector, designed to trigger on [22, 23] and identify electrons, muons, photons, and (charged and neutral) hadrons [24–26]. A global "particle-flow" (PF) algorithm [27] aims to reconstruct all individual particles in an event, combining information provided by the all-silicon inner tracker and by the crystal electromagnetic and brass-scintillator hadron calorimeters, operating inside a 3.8 T superconducting solenoid, with data from the gas-ionization muon detectors embedded in the flux-return yoke outside the solenoid. The reconstructed particles are used to build τ leptons, jets, and missing transverse momentum ($p_\mathrm{T}^\mathrm{miss}$) [28–30].

Simulated samples of signal and background events are produced at the matrix element level using various Monte Carlo (MC) event generators. The QCD multijet, Z+jets, and W+jets processes are modeled at QCD leading order (LO) accuracy using the MADGRAPH5_aMC@NLO v2.4.2 generator [31]. The vector boson samples contains decays to all flavors of quarks, and in-

clude up to 3 (4) extra partons at the matrix element level for V+jets events. Jets from the matrix element calculations and the parton shower description are matched using the MLM prescription [32]. The $t\bar{t}$ and single top quark processes are modeled at next-to-LO (NLO) using POWHEG 2.0 [33–38]. The diboson processes are modeled at LO accuracy with PYTHIA 8.226 [39]. For 2016 data-taking conditions, QCD samples are modeled with MADGRAPH5_aMC@NLO v2.2.2, and diboson samples are modeled with PYTHIA 8.205.

The differential cross sections for the Z+jets and W+jets (V+jets) samples are corrected with boson p_T-dependent functions for higher-order QCD and electroweak (EW) effects. The QCD NLO corrections are derived using MADGRAPH5_aMC@NLO, simulating W and Z production with up to two additional partons and the FXFX matching to the parton shower [40]. The EW NLO corrections are taken from theoretical calculations of Refs. [41–44]. Additionally, the total cross sections for the diboson samples are corrected to next-to-NLO (NNLO) accuracy with the MCFM 7.0 program [45].

The ggF H production process is simulated using the HJ-MINLO [35, 46–48] event generator with mass $m_H = 125\,\text{GeV}$ and including finite top quark mass effects, following the recommendation in Ref. [48]. The POWHEG [49] generator is used to model the H production through the VBF, VH, and $t\bar{t}H$ processes [47, 50, 51].

For parton showering and hadronization, the POWHEG and MADGRAPH5_aMC@NLO samples are interfaced with PYTHIA 8.205 (8.230) for 2016 (2017–2018) running conditions. The corresponding PYTHIA parameters for the underlying event description are set to the CUETP8M1 [52] (CP5 [53]) tune. For 2016 samples the parton distribution function (PDF) set NNPDF3.0 [54] is used, with either LO or NLO accuracy, corresponding to that used in the matrix element calculations, while for 2017–2018 samples NNPDF3.1 [55] at NNLO accuracy is used for all processes. The detector response is modeled with GEANT4 [56].

Reconstructed particles are clustered into jets using the anti-k_T algorithm [57, 58]. Small-radius jets are clustered with a distance parameter of 0.4 (AK4 jets). Large-radius jets arising from the decays of boosted heavy particles are reconstructed with a distance parameter of 0.8 (AK8 jets). The effect of particles from additional proton-proton interactions within the same or nearby bunch crossings (pileup) is mitigated through the charged hadron subtraction [27] and pileup-per-particle identification [59] algorithms for AK4 and AK8 jets, respectively. Additional corrections are applied to the jet energy as functions of jet pseudorapidity (η) and p_T to account for the detector response.

The H candidate is reconstructed as a single AK8 jet with $p_T > 450\,\text{GeV}$. A mix of triggers using jet p_T or a scalar sum of the jet p_T in the event is employed for online selection. At $p_T = 450\,\text{GeV}$, the online selection is 90% efficient with respect to the offline selection, reaching full efficiency by 500 GeV. The soft-drop (SD) algorithm [60] with parameters $\beta = 0$ and $z = 0.1$ is applied to the jet mass (m_{SD}) to remove soft and wide-angle radiation, which reduces the mass of jets originating from QCD background events while preserving the mass of jets originating from heavy boson decays. The range of interest is set to $40 < m_{SD} < 201\,\text{GeV}$. To match the tracker acceptance region, jets are required to have $|\eta| < 2.5$. In case of several jets in the event passing the criteria, the jet with the highest charm versus light tagging score, defined below, is taken to be the H candidate.

After the above selections, the dominant background is the QCD multijet production, which accounts for more than 95% of the expected yield and is estimated from data. The V+jets processes are significant resonant backgrounds at approximately 4%, and are estimated from simulation. The $t\bar{t}$ process constitutes a sub-dominant nonresonant background across the m_{SD}

spectrum, the shape of which is taken from simulation, while the total yield is estimated from data. Other EW processes, including diboson, triboson, and $t\bar{t}V$ processes, are estimated from simulation and found to be negligible.

Events containing leptons are vetoed to reduce SM EW backgrounds. The selection criteria for electrons, muons, and hadronic τ leptons are $p_T > 10$, 10, and 20 GeV and $|\eta| < 2.5$, 2.4, and 2.3, along with "veto", "loose", and "very loose" identification requirements [24, 28, 61], respectively. In addition, muons are required to have a relative isolation (scalar p_T sum of the PF candidates within a cone with a distance parameter of 0.4, divided by the lepton p_T) of less than 0.25. Events with $p_T^{miss} > 140$ GeV, as well as events with AK4 b-tagged jets with $p_T > 30$ GeV opposite in azimuth to the H candidate jet ($\Delta\phi(\text{AK4}, \text{AK8}) > \pi/2$), are removed to reduce the top quark background. The AK4 b jet identification is performed using the DEEPCSV DNN algorithm [62] with a working point corresponding to a 1% misidentification probability for light (u, d, s quark, or gluon) jets.

The dimensionless mass scale variable $\rho = 2\ln(m_{SD}/p_T)$ [63, 64] is used to parametrize the QCD background model (described below) as its distribution is approximately invariant versus jet p_T, unlike jet m_{SD}. A selection of $-6.0 < \rho < -2.1$ is imposed to avoid instabilities and edge effects from the SD algorithm and jet clustering [65]. The lower ρ threshold implies an upper jet p_T threshold, which is made explicit by requiring $p_T < 1200$ GeV. In simulation, less than 1% of signal events are found above this upper bound.

The N_2^1 variable [66], a ratio of energy correlation functions [67], is a powerful way to identify two-pronged signatures. However, using it for selection distorts the background jet mass distribution as a function of p_T. To mitigate this effect, the designing decorrelated taggers (DDT) technique [64], effectively a sliding selection, is applied. The selection is on $N_2^{1,DDT} \equiv N_2^1 - q_{0.26}(p_T, \rho) < 0$, where $q_{0.26}(p_T, \rho)$ is the N_2^1 value corresponding to the 26% efficiency for the QCD background, as a function of jet p_T and ρ. The target percentile is chosen to optimize the $H \to c\bar{c}$ expected significance.

Finally, jet flavor is determined by the DEEPDOUBLEX DNN algorithm [68]. The model comprises convolutional and recurrent units processing low-level features of secondary vertices and PF candidates, the outputs of which are joined with expert variables [62] in a fully connected layer. The application of feature importance ranking techniques, such as integrated gradients [69] and deep Taylor decomposition [70], indicates the key features to be the angular distances of the PF candidates from both the jet and 2-subjetiness [71] axes. The kinematic properties of the PF candidates defined relative to the parent jet have subleading importance. The model is trained to distinguish between two-pronged H-like signatures of bottom and charm flavors, as well as the QCD background, yielding two per-jet classifiers: charm versus light, referred to as DEEPDOUBLECVL (DDCvL), and charm versus bottom, referred to as DEEPDOUBLECVB (DDCvB). The performance of the two classifiers is shown, prior to any analysis-specific selection, in Fig. 1. The optimal working point, maximizing the $H \to c\bar{c}$ expected significance after all previous selections are applied, is found with respect to both classifiers at a QCD efficiency of 0.5% and a $H \to c\bar{c}$ efficiency of 20.6%. The corresponding efficiency for $H(b\bar{b})$ events is 4.8%.

The relative contributions of H production modes to the overall signal yield are 55%, 25%, and 20% for ggF, VBF, and VH, respectively. Events passing all of the selection requirements described above constitute the signal or "passing" region (SR), whereas events failing the DDCvL requirement while passing the rest, including the DDCvB requirement, constitute the control or "failing" region (CR). Both the SR and CR are subdivided into 23 evenly-spaced bins of jet m_{SD} in the range 40–201 GeV and 6 p_T bins from 450 (or 475) to 1200 GeV. Additionally, all regions

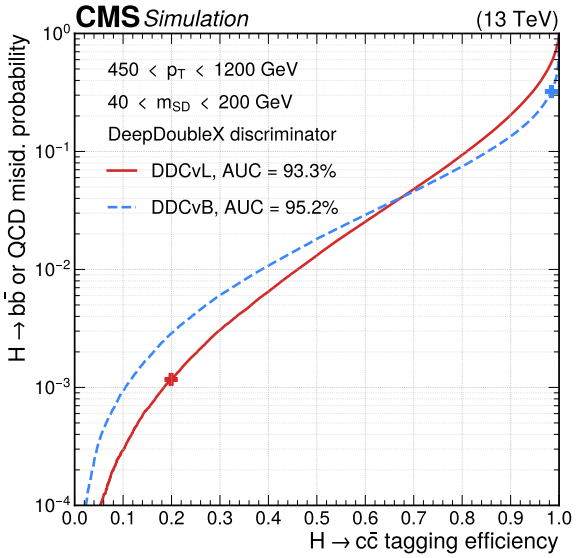

Figure 1: The DDCvL and DDCvB performance for $H \to c\bar{c}$ identification versus QCD and $H \to b\bar{b}$ processes respectively. No selection apart from the displayed m_{SD} and p_T requirements is applied. The working points used in this search are marked with a cross. The AUC is the area-under-curve metric.

are subdivided according to the three data-taking years (2016–2018).

The QCD background is not accurately predicted in simulation. Since the flavor discrimination is nearly independent of the jet p_T and mass, the ratio of the passing and failing region distributions, $R_{p/f}$, is expected to be approximately flat with respect to the jet p_T and m_{SD}. This can be exploited to obtain an SR prediction of the QCD background from the CR via an appropriate efficiency scaling. A residual difference in shapes can be accounted for by parametrizing the $R_{p/f}$ shape in the two dimensions. In order to take into account a potential mass-dependence of the flavor selection efficiency, a correction factor, $R^{QCD}_{p/f}(p_T, \rho)$, is fit to the simulated QCD background shapes. Then, a second correction factor of the same functional form, $R^{data}(p_T, \rho)$, accounts for mismodellings in simulation. Both are parametrized in terms of Bernstein polynomials [72] in p_T and ρ:

$$R(p_T, \rho) = \sum_{k=0}^{n_\rho} \sum_{\ell=0}^{n_{p_T}} a_{k,\ell} b_{\ell, n_{p_T}}(p_T) b_{k, n_\rho}(\rho), \tag{1}$$

where n_{p_T} is the degree of the polynomial in p_T, n_ρ is the degree of the polynomial in ρ, $a_{k,\ell}$ is a Bernstein coefficient, and $b_{\nu,n}$ is a Bernstein basis polynomial of degree n. The coefficients $a_{k,\ell}$ of $R^{QCD}_{p/f}(p_T, \rho)$ are determined in a fit to simulated QCD background events; $a_{k,\ell}$ of $R^{data}_{p/f}(p_T, \rho)$ are unconstrained and are determined during the maximum likelihood fit to data. The total effective $R_{p/f}$ is then expressed as:

$$R_{p/f}(p_T, \rho) = R^{QCD}_{p/f}(p_T, \rho) R^{data}(p_T, \rho). \tag{2}$$

The $R_{p/f}$ are expected to vary between data-taking years because of changes in detector conditions, and are thus fit independently for each year. The minimal degree of the polynomials necessary to fit the QCD simulation and the data is determined by a Fisher F-test [73] and found to be $(n_{p_T}, n_\rho) = (0, 2), (1, 2)$, and $(0, 2)$ for $R^{QCD}_{p/f}(p_T, \rho)$ and $(1, 0), (0, 0)$, and $(1, 0)$

for $R^{\text{data}}(p_{\text{T}}, \rho)$ for the years 2016, 2017, and 2018, respectively. Bias tests are performed with respect to the choice of parametrization, and no significant bias is found.

The V+jets processes are modeled using simulation. The differential $\text{t}\bar{\text{t}}$ contribution is taken from simulation; however the normalizations in the SR and CR are corrected via scale factors measured in a dedicated $\text{t}\bar{\text{t}}$-enriched control region. This region is adapted from the SR selection by lowering the H candidate p_{T} threshold, requiring exactly one muon, and inverting the selection requirements on $p_{\text{T}}^{\text{miss}}$ and b-tagged AK4 jets. The scale factor measurement is performed *in-situ* during the signal extraction, separately for each data-taking period. The $\text{H} \to \text{b}\bar{\text{b}}$ contribution is taken from the simulation and is fixed to the SM expectation. With an expected SR yield of a similar order to that of the $\text{H} \to \text{c}\bar{\text{c}}$ signal, its impact is negligible with respect to the overall background uncertainty.

The dominant systematic uncertainties for this search are related to the flavor tagging efficiency and jet mass shape. Corrections of the jet mass, jet mass resolution, and $N_2^{1,\text{DDT}}$ and DDCvB efficiencies are derived from data using W boson jets from semileptonic $\text{t}\bar{\text{t}}$ events. These corrections are measured independently of jet flavor, and as such are correlated among all considered resonant (H, Z, W) production and decay processes. The DDCvL misidentification efficiency of the W process is measured here as well. The corrections and their associated uncertainties are given in Table 1.

Table 1: Summary of the applied data-to-simulation scale factors for the jet mass, jet mass resolution, $N_2^{1,\text{DDT}}$ selection, and DEEPDOUBLEX selections for different data-taking periods. The jet mass correction is additive, in units of GeV.

Data period	Jet mass correction [GeV]	Jet mass resolution	$N_2^{1,\text{DDT}}$, CvB selection	CvL selection (W+jets)	CvL selection (signal)
2016	-1.17 ± 0.22	1.021 ± 0.017	0.89 ± 0.02	0.62 ± 0.09	1.15 ± 0.25
2017	-1.19 ± 0.23	1.019 ± 0.016	0.90 ± 0.02	0.64 ± 0.09	0.85 ± 0.16
2018	-0.12 ± 0.21	1.090 ± 0.031	0.92 ± 0.02	0.72 ± 0.08	0.74 ± 0.20

The efficiency of the DDCVL selection for the signal processes is estimated using data and simulation samples enriched in $\text{c}\bar{\text{c}}$ pairs from gluon splitting [62]. Signal-like events are selected by requiring each of the two SD subjets of an AK8 jet to contain a muon, targeting semileptonic decays of b/c hadrons. The efficiency is extracted from a template fit to the combined mass of all matched secondary vertices; the measured correction factors are given in Table 1. The relative uncertainty of the misidentification efficiency of $\text{b}\bar{\text{b}}$ decays is assigned to be 30%.

Other systematic uncertainties are assigned to cover potential mismodeling of the H signal, in particular for the ggF and VBF production modes [48], and higher-order corrections to the W and Z processes [44]. Finally, systematic uncertainties for experimental effects, including jet energy scale and resolution [74], trigger and veto efficiencies [75, 76], variations in the measured pileup [77], finite simulated sample size [78], and an integrated luminosity measurement [79–81], are also included, but are found to have a comparatively small effect.

The parameter of interest in this analysis is the signal strength μ_{H} or μ_{Z}, defined as the ratio of the observed to the SM expected H or Z boson production cross section times the $\text{H} \to \text{c}\bar{\text{c}}$ or $\text{Z} \to \text{c}\bar{\text{c}}$ branching fraction, respectively. These parameters are extracted from a binned (m_{SD}, p_{T}) maximum likelihood fit to the observed data, where the expected value is the sum of the signal contribution (scaled by the signal strength parameter) and the background contributions, each modified by nuisance parameters to account for the previously discussed systematic effects. The magnitude of each systematic uncertainty is encoded in the likelihood model as an additional constraint, treated according to the frequentist paradigm [82]. The fit is performed

simultaneously across all subdivisions of the SR and CR described previously, as well as the per-year $t\bar{t}$ background enriched CRs.

To validate the analysis strategy, as well as to confirm the presence of $Z \to c\bar{c}$ decays, the Z signal strength μ_Z is measured via a profile likelihood fit, treating μ_H as a nuisance parameter, and is found to be $1.00^{+0.17}_{-0.14}$ (syst) $\pm$ 0.08 (theo) $\pm$ 0.06 (stat). This corresponds to an excess, both observed and expected, over the $\mu_Z = 0$ hypothesis with a significance of well over 5 standard deviations. The precision of the μ_Z measurement is primarily limited by the systematic uncertainty in the DDCvL signal tagging efficiency. The subleading uncertainty comes from the modeling of the Z+jets production cross section.

For the extraction of μ_H, since the Z cross section has been measured in leptonic decay channels and found to agree with theoretical predictions within 5% in this p_T regime [83] and since the $Z \to c\bar{c}$ branching ratio is known to 2% precision [84], we fix $\mu_Z \equiv 1$, constraining the expected Z contribution to be within the applicable uncertainties of its SM value. This serves to further constrain *in-situ* the DDCvL signal tagging efficiency uncertainty. The measured efficiencies are compatible with the values quoted in Table 1 and have approximately 30% lower uncertainty.

An observed (expected) upper limit is placed on the signal strength μ_H using the profile likelihood ratio test statistic [82], CL_s criterion [85, 86], and asymptotic formulae [87], and found to be 47 (39) at 95% confidence level. For the best fit value of $\mu_H = 9.4^{+20.3}_{-19.9}$, the total m_{SD} distributions in the passing and failing regions are shown in Fig. 2, and a breakdown of the sources of uncertainty affecting the measurement is shown in Table 2. Tabulated results are provided in the HEPData record for this analysis [88].

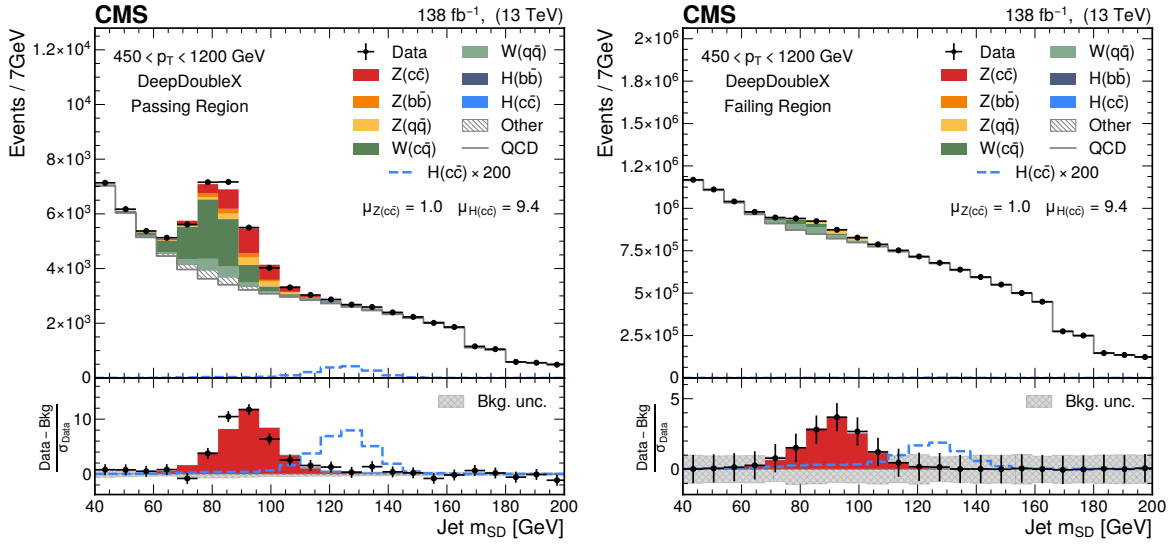

Figure 2: The observed and fitted m_{SD} distributions for the passing (left) and failing (right) regions, combining all p_T categories and the three data-taking years. The fit is performed under the signal-plus-background hypothesis with a single inclusive $H(c\bar{c})$ signal strength parameter. The $t\bar{t}$ background yields and the QCD background yields and shapes are estimated from data. The $t\bar{t}$ process constitutes the majority of contributions labeled "Other". The dashed line represents the $H \to c\bar{c}$ expectation, multiplied by a factor of 200. The step-like features at 166 and 180 GeV are due to m_{SD} bins excluded from the ρ acceptance region. The lower panel shows the residual difference between the data and the overall background (excluding $Z \to c\bar{c}$), divided by the statistical uncertainty in the data. The near perfect model agreement with data in the failing region (right) is by construction.

Table 2: Sources of uncertainty in the measurement of the signal strength $\mu_{\mathrm{H}} = 9.4^{+20.3}_{-19.9}$, and their observed impact ($\Delta\mu_{\mathrm{H}}$) in the fit to the full data set. The impact of each uncertainty is evaluated by computing the uncertainty excluding that source and subtracting it in quadrature from the total uncertainty. The total uncertainty does not match the sum in quadrature of each source because of correlations among the components.

Uncertainty source	$\Delta\mu_{\mathrm{H}}$	
Statistical	+16.7	-16.6
Signal extraction	+14.2	-14.1
QCD pass-fail ratio (data correction)	+7.4	-7.4
$\mathrm{t\bar{t}}$ normalization and misidentification	+0.9	-0.7
Systematic	+10.5	-10.4
QCD pass-fail ratio (simulation)	+9.7	-9.8
Flavor (mis-)tagging efficiency	+1.7	-2.2
Simulated sample size	+4.2	-3.6
Other experimental uncertainties	+2.1	-1.4
Theoretical	+3.9	-1.6
V+jets modeling	+2.3	-1.2
H modeling	+3.2	-1.0
Total	+20.3	-19.9

In conclusion, a search for standard model (SM) Z and Higgs bosons produced with transverse momenta greater than 450 GeV and decaying to charm quark-antiquark ($\mathrm{c\bar{c}}$) pairs has been performed in a data sample corresponding to an integrated luminosity of 138 fb^{-1} at $\sqrt{s} =$ 13 TeV. New algorithms based on deep neural networks have been developed to identify jets originating from charm quark pairs. The $\mathrm{Z} \to \mathrm{c\bar{c}}$ process is observed in association with jets at a hadron collider for the first time, with a signal strength of $1.00^{+0.19}_{-0.17}$ relative to the SM prediction. An observed (expected) upper limit on the product of the Higgs boson production cross section and branching fraction to $\mathrm{c\bar{c}}$ of 47 (39) times the SM expectation is set at 95% confidence level.

References

[1] ATLAS Collaboration, "Observation of a new particle in the search for the standard model Higgs boson with the ATLAS detector at the LHC", *Phys. Lett. B* **716** (2012) 1, doi:10.1016/j.physletb.2012.08.020, arXiv:1207.7214.

[2] CMS Collaboration, "Observation of a new boson at a mass of 125 GeV with the CMS experiment at the LHC", *Phys. Lett. B* **716** (2012) 30, doi:10.1016/j.physletb.2012.08.021, arXiv:1207.7235.

[3] CMS Collaboration, "Observation of a new boson with mass near 125 GeV in pp collisions at $\sqrt{s} = 7$ and 8 TeV", *JHEP* **06** (2013) 081, doi:10.1007/JHEP06(2013)081, arXiv:1303.4571.

[4] CMS Collaboration, "Observation of the Higgs boson decay to a pair of τ leptons with the CMS detector", *Phys. Lett. B* **779** (2018) 283, doi:10.1016/j.physletb.2018.02.004, arXiv:1708.00373.

[5] ATLAS Collaboration, "Measurements of Higgs boson production cross-sections in the $H \to \tau^+\tau^-$ decay channel in pp collisions at $\sqrt{s} = 13$ TeV with the ATLAS detector", *JHEP* **08** (2022) 175, doi:10.1007/JHEP08(2022)175, arXiv:2201.08269.

[6] CMS Collaboration, "Observation of $t\bar{t}H$ production", *Phys. Rev. Lett.* **120** (2018) 231801, doi:10.1103/PhysRevLett.120.231801, arXiv:1804.02610.

[7] ATLAS Collaboration, "Observation of Higgs boson production in association with a top quark pair at the LHC with the ATLAS detector", *Phys. Lett. B* **784** (2018) 173, doi:10.1016/j.physletb.2018.07.035, arXiv:1806.00425.

[8] ATLAS Collaboration, "Observation of $H \to b\bar{b}$ decays and VH production with the ATLAS detector", *Phys. Lett. B* **786** (2018) 59, doi:10.1016/j.physletb.2018.09.013, arXiv:1808.08238.

[9] CMS Collaboration, "Observation of Higgs boson decay to bottom quarks", *Phys. Rev. Lett.* **121** (2018) 121801, doi:10.1103/PhysRevLett.121.121801, arXiv:1808.08242.

[10] CMS Collaboration, "Search for the Higgs boson decaying to two muons in proton-proton collisions at $\sqrt{s} = 13$ TeV", *Phys. Rev. Lett.* **122** (2019) 021801, doi:10.1103/PhysRevLett.122.021801, arXiv:1807.06325.

[11] ATLAS Collaboration, "A search for the dimuon decay of the standard model Higgs boson with the ATLAS detector", *Phys. Lett. B* **812** (2021) 135980, doi:10.1016/j.physletb.2020.135980, arXiv:2007.07830.

[12] ATLAS Collaboration, "Search for the dimuon decay of the Higgs boson in pp collisions at $\sqrt{s} = 13$ TeV with the ATLAS detector", *Phys. Rev. Lett.* **119** (2017) 051802, doi:10.1103/PhysRevLett.119.051802, arXiv:1705.04582.

[13] CMS Collaboration, "Evidence for Higgs boson decay to a pair of muons", *JHEP* **01** (2021) 148, doi:10.1007/JHEP01(2021)148, arXiv:2009.04363.

[14] CMS Collaboration, "Performance of deep tagging algorithms for boosted double quark jet topology in proton-proton collisions at 13 TeV with the Phase-0 CMS detector", CMS Detector Performance Note CMS-DP-2018-046, 2018.

[15] ATLAS Collaboration, "Search for the decay of the Higgs boson to charm quarks with the ATLAS experiment", *Phys. Rev. Lett.* **120** (2018) 211802, doi:10.1103/PhysRevLett.120.211802, arXiv:1802.04329.

[16] ATLAS Collaboration, "Direct constraint on the Higgs-charm coupling from a search for Higgs boson decays into charm quarks with the ATLAS detector", *Eur. Phys. J. C* **82** (2022) 717, doi:10.1140/epjc/s10052-022-10588-3, arXiv:2201.11428.

[17] CMS Collaboration, "A search for the standard model Higgs boson decaying to charm quarks", *JHEP* **03** (2020) 131, doi:10.1007/JHEP03(2020)131, arXiv:1912.01662.

[18] CMS Collaboration, "Search for Higgs boson decay to a charm quark-antiquark pair in proton-proton collisions at $\sqrt{s} = 13$ TeV", 2022. arXiv:2205.05550. Submitted to *Phys. Rev. Lett.*

[19] CMS Collaboration, "Inclusive search for a highly boosted Higgs boson decaying to a bottom quark-antiquark pair", *Phys. Rev. Lett.* **120** (2018) 071802, doi:10.1103/PhysRevLett.120.071802, arXiv:1709.05543.

[20] CMS Collaboration, "Inclusive search for highly boosted Higgs bosons decaying to bottom quark-antiquark pairs in proton-proton collisions at $\sqrt{s} = 13\,\text{TeV}$", *JHEP* **12** (2020) 085, doi:10.1007/JHEP12(2020)085, arXiv:2006.13251.

[21] CMS Collaboration, "The CMS experiment at the CERN LHC", *JINST* **3** (2008) S08004, doi:10.1088/1748-0221/3/08/S08004.

[22] CMS Collaboration, "The CMS trigger system", *JINST* **12** (2017) P01020, doi:10.1088/1748-0221/12/01/P01020, arXiv:1609.02366.

[23] CMS Collaboration, "Performance of the CMS Level-1 trigger in proton-proton collisions at $\sqrt{s} = 13\,\text{TeV}$", *JINST* **15** (2020) P10017, doi:10.1088/1748-0221/15/10/P10017, arXiv:2006.10165.

[24] CMS Collaboration, "Electron and photon reconstruction and identification with the CMS experiment at the CERN LHC", *JINST* **16** (2021) P05014, doi:10.1088/1748-0221/16/05/P05014, arXiv:2012.06888.

[25] CMS Collaboration, "Performance of the CMS muon detector and muon reconstruction with proton-proton collisions at $\sqrt{s} = 13\,\text{TeV}$", *JINST* **13** (2018) P06015, doi:10.1088/1748-0221/13/06/P06015, arXiv:1804.04528.

[26] CMS Collaboration, "Description and performance of track and primary-vertex reconstruction with the CMS tracker", *JINST* **9** (2014) P10009, doi:10.1088/1748-0221/9/10/P10009, arXiv:1405.6569.

[27] CMS Collaboration, "Particle-flow reconstruction and global event description with the CMS detector", *JINST* **12** (2017) P10003, doi:10.1088/1748-0221/12/10/P10003, arXiv:1706.04965.

[28] CMS Collaboration, "Performance of reconstruction and identification of τ leptons decaying to hadrons and ν_τ in pp collisions at $\sqrt{s} = 13\,\text{TeV}$", *JINST* **13** (2018) P10005, doi:10.1088/1748-0221/13/10/P10005, arXiv:1809.02816.

[29] CMS Collaboration, "Jet energy scale and resolution in the CMS experiment in pp collisions at 8 TeV", *JINST* **12** (2017) P02014, doi:10.1088/1748-0221/12/02/P02014, arXiv:1607.03663.

[30] CMS Collaboration, "Performance of missing transverse momentum reconstruction in proton-proton collisions at $\sqrt{s} = 13\,\text{TeV}$ using the CMS detector", *JINST* **14** (2019) P07004, doi:10.1088/1748-0221/14/07/P07004, arXiv:1903.06078.

[31] J. Alwall et al., "The automated computation of tree-level and next-to-leading order differential cross sections, and their matching to parton shower simulations", *JHEP* **07** (2014) 079, doi:10.1007/JHEP07(2014)079, arXiv:1405.0301.

[32] J. Alwall et al., "Comparative study of various algorithms for the merging of parton showers and matrix elements in hadronic collisions", *Eur. Phys. J. C* **53** (2008) 473, doi:10.1140/epjc/s10052-007-0490-5, arXiv:0706.2569.

[33] P. Nason, "A new method for combining NLO QCD with shower Monte Carlo algorithms", *JHEP* **11** (2004) 040, doi:10.1088/1126-6708/2004/11/040, arXiv:hep-ph/0409146.

[34] S. Frixione, P. Nason, and G. Ridolfi, "A positive-weight next-to-leading-order Monte Carlo for heavy flavour hadroproduction", *JHEP* **09** (2007) 126, doi:10.1088/1126-6708/2007/09/126, arXiv:0707.3088.

[35] S. Frixione, P. Nason, and C. Oleari, "Matching NLO QCD computations with parton shower simulations: the POWHEG method", *JHEP* **11** (2007) 070, doi:10.1088/1126-6708/2007/11/070, arXiv:0709.2092.

[36] S. Alioli, P. Nason, C. Oleari, and E. Re, "A general framework for implementing NLO calculations in shower Monte Carlo programs: the POWHEG BOX", *JHEP* **06** (2010) 043, doi:10.1007/JHEP06(2010)043, arXiv:1002.2581.

[37] E. Re, "Single-top Wt-channel production matched with parton showers using the POWHEG method", *Eur. Phys. J. C* **71** (2011) 1547, doi:10.1140/epjc/s10052-011-1547-z, arXiv:1009.2450.

[38] R. Frederix, E. Re, and P. Torrielli, "Single-top *t*-channel hadroproduction in the four-flavour scheme with POWHEG and aMC@NLO", *JHEP* **09** (2012) 130, doi:10.1007/JHEP09(2012)130, arXiv:1207.5391.

[39] T. Sjöstrand et al., "An introduction to PYTHIA 8.2", *Comput. Phys. Commun.* **191** (2015) 159, doi:10.1016/j.cpc.2015.01.024, arXiv:1410.3012.

[40] R. Frederix and S. Frixione, "Merging meets matching in MC@NLO", *JHEP* **12** (2012) 061, doi:10.1007/JHEP12(2012)061, arXiv:1209.6215.

[41] S. Kallweit et al., "NLO electroweak automation and precise predictions for W+multijet production at the LHC", *JHEP* **04** (2015) 012, doi:10.1007/JHEP04(2015)012, arXiv:1412.5157.

[42] S. Kallweit et al., "NLO QCD+EW automation and precise predictions for V+multijet production", in *50th Rencontres de Moriond, QCD and high energy interactions*, p. 121. 2015. arXiv:1505.05704.

[43] S. Kallweit et al., "NLO QCD+EW predictions for V+jets including off-shell vector-boson decays and multijet merging", *JHEP* **04** (2016) 021, doi:10.1007/JHEP04(2016)021, arXiv:1511.08692.

[44] J. M. Lindert et al., "Precise predictions for V+jets dark matter backgrounds", *Eur. Phys. J. C* **77** (2017) 829, doi:10.1140/epjc/s10052-017-5389-1, arXiv:1705.04664.

[45] J. M. Campbell and R. K. Ellis, "MCFM for the Tevatron and the LHC", *Nucl. Phys. Proc. Suppl.* **205-206** (2010) 10, doi:10.1016/j.nuclphysbps.2010.08.011, arXiv:1007.3492.

[46] K. Hamilton, P. Nason, C. Oleari, and G. Zanderighi, "Merging H/W/Z + 0 and 1 jet at NLO with no merging scale: a path to parton shower + NNLO matching", *JHEP* **05** (2013) 082, doi:10.1007/JHEP05(2013)082, arXiv:1212.4504.

[47] G. Luisoni, P. Nason, C. Oleari, and F. Tramontano, "HW$^{\pm}$/HZ+0 and 1 jet at NLO with the POWHEG box interfaced to GoSam and their merging within MINLO", *JHEP* **10** (2013) 083, doi:10.1007/JHEP10(2013)083, arXiv:1306.2542.

[48] K. Becker et al., "Precise predictions for boosted Higgs production", 2020. arXiv:2005.07762.

[49] E. Bagnaschi, G. Degrassi, P. Slavich, and A. Vicini, "Higgs production via gluon fusion in the POWHEG approach in the SM and in the MSSM", *JHEP* **02** (2012) 088, doi:10.1007/JHEP02(2012)088, arXiv:1111.2854.

[50] P. Nason and C. Oleari, "NLO Higgs boson production via vector-boson fusion matched with shower in POWHEG", *JHEP* **02** (2010) 037, doi:10.1007/JHEP02(2010)037, arXiv:0911.5299.

[51] H. B. Hartanto, B. Jäger, L. Reina, and D. Wackeroth, "Higgs boson production in association with top quarks in the POWHEG BOX", *Phys. Rev. D* **91** (2015) 094003, doi:10.1103/PhysRevD.91.094003, arXiv:1501.04498.

[52] CMS Collaboration, "Event generator tunes obtained from underlying event and multiparton scattering measurements", *Eur. Phys. J. C* **76** (2016) 155, doi:10.1140/epjc/s10052-016-3988-x, arXiv:1512.00815.

[53] CMS Collaboration, "Extraction and validation of a new set of CMS PYTHIA8 tunes from underlying-event measurements", *Eur. Phys. J. C* **80** (2020) 4, doi:10.1140/epjc/s10052-019-7499-4, arXiv:1903.12179.

[54] NNPDF Collaboration, "Parton distributions for the LHC run II", *JHEP* **04** (2015) 040, doi:10.1007/JHEP04(2015)040, arXiv:1410.8849.

[55] NNPDF Collaboration, "Parton distributions from high-precision collider data", *Eur. Phys. J. C* **77** (2017) 663, doi:10.1140/epjc/s10052-017-5199-5, arXiv:1706.00428.

[56] GEANT4 Collaboration, "GEANT4—a simulation toolkit", *Nucl. Instrum. Meth. A* **506** (2003) 250, doi:10.1016/S0168-9002(03)01368-8.

[57] M. Cacciari, G. P. Salam, and G. Soyez, "The anti-k_{T} jet clustering algorithm", *JHEP* **04** (2008) 063, doi:10.1088/1126-6708/2008/04/063, arXiv:0802.1189.

[58] M. Cacciari, G. P. Salam, and G. Soyez, "FastJet user manual", *Eur. Phys. J. C* **72** (2012) 1896, doi:10.1140/epjc/s10052-012-1896-2, arXiv:1111.6097.

[59] D. Bertolini, P. Harris, M. Low, and N. Tran, "Pileup per particle identification", *JHEP* **10** (2014) 059, doi:10.1007/JHEP10(2014)059, arXiv:1407.6013.

[60] A. J. Larkoski, S. Marzani, G. Soyez, and J. Thaler, "Soft drop", *JHEP* **05** (2014) 146, doi:10.1007/JHEP05(2014)146, arXiv:1402.2657.

[61] CMS Collaboration, "Performance of the reconstruction and identification of high-momentum muons in proton-proton collisions at $\sqrt{s} = 13\,\mathrm{TeV}$", *JINST* **15** (2020) P02027, doi:10.1088/1748-0221/15/02/P02027, arXiv:1912.03516.

[62] CMS Collaboration, "Identification of heavy-flavour jets with the CMS detector in pp collisions at 13 TeV", *JINST* **13** (2018) P05011, doi:10.1088/1748-0221/13/05/P05011, arXiv:1712.07158.

[63] M. Dasgupta, A. Fregoso, S. Marzani, and G. P. Salam, "Towards an understanding of jet substructure", *JHEP* **09** (2013) 029, doi:10.1007/JHEP09(2013)029, arXiv:1307.0007.

[64] J. Dolen et al., "Thinking outside the ROCs: Designing decorrelated taggers (DDT) for jet substructure", *JHEP* **05** (2016) 156, doi:10.1007/JHEP05(2016)156, arXiv:1603.00027.

[65] ATLAS Collaboration, "Measurement of soft-drop jet observables in pp collisions with the ATLAS detector at $\sqrt{s} = 13$ TeV", *Phys. Rev. D* **101** (2020) 052007, doi:10.1103/PhysRevD.101.052007, arXiv:1912.09837.

[66] I. Moult, L. Necib, and J. Thaler, "New angles on energy correlation functions", *JHEP* **12** (2016) 153, doi:10.1007/JHEP12(2016)153, arXiv:1609.07483.

[67] A. J. Larkoski, G. P. Salam, and J. Thaler, "Energy correlation functions for jet substructure", *JHEP* **06** (2013) 108, doi:10.1007/JHEP06(2013)108, arXiv:1305.0007.

[68] CMS Collaboration, "Performance of the mass-decorrelated DeepDoubleX classifier for double-b and double-c large-radius jets with the CMS detector", CMS Detector Performance Note CMS-DP-2022-041, 2022.

[69] M. Sundararajan, A. Taly, and Q. Yan, "Axiomatic attribution for deep networks", in *Proceedings of the 34th International Conference on Machine Learning*, p. 3319. PMLR, 2017. arXiv:1703.01365.

[70] G. Montavon et al., "Explaining nonlinear classification decisions with deep Taylor decomposition", *Pattern Recognit.* **65** (2017) 211, doi:10.1016/j.patcog.2016.11.008, arXiv:1512.02479.

[71] J. Thaler and K. Van Tilburg, "Identifying boosted objects with N-subjettiness", *JHEP* **03** (2011) 015, doi:10.1007/JHEP03(2011)015, arXiv:1011.2268.

[72] S. Bernstein, "Démonstration du théorème de Weierstrass fondée sur le calcul des probabilités", *Comm. Kharkov Math. Soc.* **13** (1912) 01.

[73] R. A. Fisher, "On the interpretation of χ^2 from contingency tables, and the calculation of P", *J. R. Stat. Soc.* **85** (1922) 87, doi:10.2307/2340521.

[74] CMS Collaboration, "Jet energy scale and resolution performance with 13 TeV data collected by CMS in 2016–2018", CMS Detector Performance Note CMS-DP-2020-019, 2020.

[75] CMS Collaboration, "Performance of heavy flavour identification algorithms in proton-proton collisions at 13 TeV at the CMS experiment", CMS Detector Performance Note CMS-DP-2017-012, 2017.

[76] CMS Collaboration, "Performance of b tagging algorithms in proton-proton collisions at 13 TeV with Phase 1 CMS detector", CMS Detector Performance Note CMS-DP-2018-033, 2018.

[77] CMS Collaboration, "Performance of the pile up jet identification in CMS for Run 2", CMS Detector Performance Note CMS-DP-2020-020, 2020.

[78] R. J. Barlow and C. Beeston, "Fitting using finite Monte Carlo samples", *Comput. Phys. Commun.* **77** (1993) 219, doi:10.1016/0010-4655(93)90005-W.

[79] CMS Collaboration, "Precision luminosity measurement in proton-proton collisions at $\sqrt{s} = 13$ TeV in 2015 and 2016 at CMS", *Eur. Phys. J. C* **81** (2021) 800, doi:10.1140/epjc/s10052-021-09538-2, arXiv:2104.01927.

[80] CMS Collaboration, "CMS luminosity measurement for the 2017 data-taking period at $\sqrt{s} = 13$ TeV", CMS Physics Analysis Summary CMS-PAS-LUM-17-004, 2018.

[81] CMS Collaboration, "CMS luminosity measurement for the 2018 data-taking period at $\sqrt{s} = 13$ TeV", CMS Physics Analysis Summary CMS-PAS-LUM-18-002, 2019.

[82] The ATLAS Collaboration, The CMS Collaboration, The LHC Higgs Combination Group, "Procedure for the LHC Higgs boson search combination in Summer 2011", Technical Report CMS-NOTE-2011-005, ATL-PHYS-PUB-2011-11, 2011.

[83] CMS Collaboration, "Measurement of the Z boson differential production cross section using its invisible decay mode ($Z \to \nu\bar{\nu}$) in proton-proton collisions at $\sqrt{s} = 13$ TeV", *JHEP* **05** (2021) 205, doi:10.1007/JHEP05(2021)205, arXiv:2012.09254.

[84] Particle Data Group, "Review of Particle Physics", *PTEP* **2022** (2022) 083C01, doi:10.1093/ptep/ptac097.

[85] T. Junk, "Confidence level computation for combining searches with small statistics", *Nucl. Instrum. Meth. A* **434** (1999) 435, doi:10.1016/S0168-9002(99)00498-2, arXiv:hep-ex/9902006.

[86] A. L. Read, "Presentation of search results: the CL_s technique", *J. Phys. G* **28** (2002) 2693, doi:10.1088/0954-3899/28/10/313.

[87] G. Cowan, K. Cranmer, E. Gross, and O. Vitells, "Asymptotic formulae for likelihood-based tests of new physics", *Eur. Phys. J. C* **71** (2011) 1554, doi:10.1140/epjc/s10052-011-1554-0, arXiv:1007.1727. [Erratum: doi:10.1140/epjc/s10052-013-2501-z].

[88] "HEPData record for this analysis", 2022. doi:10.17182/hepdata.NNNNN.